Photoluminescence Emission Induced by Localized States in Halide Passivated Colloidal Two-Dimensional WS_2 Nanoflakes

Rosanna Mastria,[1] Anna Loiudice,[2] Jan Vávra,[2] Concetta Nobile,[1] Riccardo Scarfiello,[1] P. Davide Cozzoli,[1,3,4] Nicola Sestu,[5] Daniela Marongiu,[5] Francesco Quochi,[5] Raffaella Buonsanti,[2] Michele Saba,[5] Arrigo Calzolari,[6] Aurora Rizzo[1]**

[1]CNR NANOTEC - Institute of Nanotecnology, Polo di Nanotecnologia, c/o Campus Ecotekne, Via Monteroni, 73100 Lecce, Italy;

[2]Laboratory of Nanochemistry for Energy (LNCE), Department of Chemical Sciences and Engineering, École Polytechnique Fédérale de Lausanne, Sion, CH-1950, Switzerland

[3]Dipartimento di Matematica e Fisica "E. De Giorgi", Università del Salento, Via per Arnesano, 73100 Lecce, Italy.

[4]UdR INSTM di Lecce, c/o, Università del Salento, Campus Ecotekne, via Arnesano, 73100 Lecce, Italy.

[5]Dipartimento di Fisica, Università di Cagliari, I-09042 Monserrato, Italy

[6]Istituto Nanoscienze, CNR-NANO, S3 Center, Via Campi 213/a, 41125 Modena, Italy

KEYWORDS: 2D transition metal dichalcogenides, colloidal WS_2, WS_2 ink, halide passivation, photoluminescence, localized states, defect engineering.

ABSTRACT: Engineering physicochemical properties of two-dimensional transition metal dichalcogenide (2D-TMD) materials by surface manipulation is essential for their practical and large-scale application especially for colloidal 2D-TMDs that are plagued by the unintentional formation of structural defects during the synthetic procedure. However, the available methods to manage surface states of 2D-TMDs in solution-phase are still limited hampering the production of high quality colloidal 2D-TMD inks to be straightforwardly assembled into actual devices. Here, we demonstrate an efficient solution-phase strategy to passivate surface defect states of colloidally synthetized WS_2 nanoflakes with halide ligands, resulting in the activation of the photoluminescence emission. Photophysical investigation and density functional theory calculations suggest that halide atoms enable the suppression of non-radiative recombination through the elimination deep gap trap states, and introduce localized states in the energy band structure from which excitons efficiently recombine. Halide passivated WS_2 nanoflakes importantly preserve colloidal stability and photoluminescence emission after several weeks of storing in ambient atmosphere, corroborating the potential of our developed 2D-TMD inks.

Two-dimensional transition metal dichalcogenides are at the forefront of materials science innovation holding great promise for next-generation semiconductor devices.[1–4] Composition, thickness, structure and surface chemistry of 2D-TMDs affect their optoelectronic properties, providing opportunities to design semiconductor materials engineered towards specific applications.[5–8] To this end, a great deal of efforts have been devoted to develop synthetic methods or post-synthetic procedures targeting the production of high quality 2D-TMD crystals with tailored photophysical properties. Herein, advances in solution-based synthetic approaches have opened the way towards large-scale and low-cost production of inks consisting of 2D-TMDs that can be potentially printed or embedded into functional films or composites in a facile and straightforward way.[9–12] Liquid phase exfoliation can easily produce a wide range of 2D-TMD inks at low cost but the limited control over the exfoliation process results in a broad distribution of crystal thickness and lateral dimension, hence

the need for tedious post production process (i.e. gradient centrifugation) to improve the monodispersity of the sample.[13,14] The surfactant assisted colloidal approaches for 2D-TMD synthesis, although still in its early stages, provide key advantages over other existing methods combining both mild synthetic condition and precise control over 2D-TMD composition, geometry and crystal structure.[15,16] Colloidal approach has been proven successful to synthesize to date a wide range of solution-processable 2D-TMDs with mono to few layer thicknesses,[17] controlled lateral size[18] and crystal phase.[19,20] The photophysical properties of colloidal 2D-TMDs, however, are nearly unexplored and the impact of structural defect and/or defect engineering on their optical and electronic properties is still poorly understood, hampering a widespread application of this promising synthetic approach.[21]

Approaching mono-to-few-layer structure of TMDs involves indirect-to-direct bandgap transition[22–26] and a decrease in dielectric screening[27] resulting in an optical response dominated by excitons with strong Coulomb interaction and, at least in principle, high photoluminescence quantum yield (PLQY). However, as synthesized colloidal 2D-TMDs, similarly to 2D-TMDs obtained with other methods, are characterized by ultrafast non-radiative recombination and extremely poor PLQY at room temperature.[23,28] Photoluminescence (PL) suppression in nanostructures with large surface-to-volume ratio, as in the case of 2D-TMDs, is often ascribed to large non-radiative recombination rates at surface states, an issue compounded by very effective Auger process that help both defect trapping and non-radiative recombination.[28,29] In colloidal 2D-TMDs, due to the volatile nature of chalcogen precursor used for the synthesis, surface defects mainly consist of chalcogen vacancies.[18,30] Such defects have been held responsible for the appearance of deep in-gap energy levels causing non-radiative electron-hole recombination, with detrimental effects on PL emission.[31,32] As a result, a high density of chalcogen vacancies hinders the extensive use of 2D-TMDs in optoelectronic platforms, for which the development of an effective strategy to engineer defects and to restore the ideal band structure suppressing in-gap trap states is essential.

Surface chemistry manipulation is a powerful tool to manage the extended surface of 2D-TMDs, to heal defects and therefore to control the structure of energy levels, enabling future opportunities for optoelectronic device applications.[6] Furthermore, substituents play an important role in 2D-TMD recombination processes creating localization centers that are responsible of a large number of localization-induced optical phenomena that could be exploited to further engineer the optical response of colloidal 2D-TMDs.[33] In previous reports, passivation of chalcogen vacancies of CVD grown or mechanically exfoliated 2D-TMDs have been achieved by performing post-deposition treatments with superacid molecules or hydrohalic acid, which are able to fill chalcogen vacancies, providing additional chalcogen atoms or substitutional heteroatoms, respectively, resulting in the enhancement of photoluminescence emission.[34,35] However, such post deposition approaches preclude any solution processability of passivated colloidal 2D-TMDs as well as any possibility of scalability. On the other hand, solution-phase passivation protocols developed for metal chalcogenides colloidal quantum dots are not effective for 2D-TMDs because of their different structure: 2D-TMDs are characterised by chalcogen-rich surfaces, i.e. unsaturated metal cations are not well-exposed to the external environment, while metal chalcogenides quantum dots exhibit metal-rich surfaces that easily react in passivating solutions.[36,37]

The ideal chemical passivation scheme for colloidal 2D-TMDs should rely on a solution-phase approach ensuring an easy access to surface states, for an improved effectiveness of the treatment, while preserving colloidal stability and solution processability. Furthermore, it should involve small molecules able to reach hard-to-access sites into individual monolayer flake.

Here, we explore monovalent halide ligands (scheme in Figure 1a) to passivate sulfur vacancies in colloidal WS_2 nanoflakes (NFs) preserving their colloidal stability. Exploiting the strong affinity of halide ligands toward non-passivated metal cations as well as their small size,[38,39] we are able to effectively passivate unsaturated metal atoms resulting in the activation of PL emission that otherwise is negligible in the pristine colloidal WS_2 NFs. Furthermore, the investigation of charge-carrier relaxation pathways in halide passivated WS_2 NFs achieved through the combination of

photoluminescence excitation (PLE) and time-resolved PL measurements reveals that halide ligands introduce high-energy localized states. Such localized states are responsible of capture events that hinder intervalley scattering and promote high-energy photon emission, thus assuming a leading role during recombination processes. Finally, Ab initio density functional theory (DFT) simulations elucidate the effect of the halide ligands on the electronic structure of WS_2 NFs and demonstrate that halide atoms act as aliovalent substituents able to saturate dangling bond states originated from chalcogen vacancies and to restore the band gap of the undefective WS_2 crystals.

These results represent a successful paradigm for the tuning of fundamental properties of colloidal 2D-TMDs and provide important insights into the understanding of excitonic phenomena associated with defect and defect passivation in colloidal 2D-TMDs.

RESULTS AND DISCUSSION

Passivation of colloidal WS_2 nanoflakes with halide ligands

Colloidal WS_2 NFs have been synthesized by exploiting an improved sacrificial-conversion route that relies on a gradual solution-phase sulfidation of $W_{18}O_{49}$ colloidal carved nanorods in a surfactant media, toward a complete conversion of carved nanorods in WS_2 nanoflakes.[40] The surfactants are essential to drive the in-plane nucleation and growth of two-dimensional WS_2 NFs[15] as well as to impart colloidal stability to NFs, overcoming their natural tendency to stack through van der Waals interactions, which emerged as the major challenge for other liquid-phase preparation methods (e.g., chemical exfoliation). Transmission electron microscopy (TEM) analysis on as prepared samples suggests that the final product consists in WS_2 bundles, with lateral mean size of about 50 nm, composed of smaller single and few-layer WS_2 NFs characterized by the coexistence of the metallic 1T' and the semiconducting 2H crystal structures.[12]

Starting from as-prepared colloidal WS_2 NFs (Figure 2a-b), we performed halide passivation upon a mild sonication in a low energy density sonication bath of a dispersion of colloidal WS_2 NFs in a N-Methylformamide (NMF) solution of methylammonium halide salts. After the treatment, WS_2 NFs

exhibit a very high solution stability in NMF (Figure S1), which suggests a stabilization through electrostatic repulsion. Indeed, we expect that negative halide anions bound unpassivated metal atoms in correspondence of chalcogen vacancies, while methylammonium cations, due to their high solvation energy, act as counterions and form a diffuse layer around NFs.[39,41,42] NMF represents the best choice among the suitable solvents for solution stabilization of WS_2 NFs since it exhibits an extraordinarily high dielectric constant (ε ~ 182), essential to stabilize nanocrystals capped with charged inorganic species.[39] Importantly, even in presence of methylammonium halide salts, and after prolonged sonication, NMF did not exhibits any signal of degradation or PL emission, unlike to other polar solvents commonly used in 2D-TMDs liquid exfoliation that exhibit PL emission after sonication, such as N-methyl-2-pyrrolidone.[43] In order to demonstrate the viability of our approach, methylammonium iodide (MAI), methylammonium bromide (MABr), and methylammonium chloride (MACl) have been selected as halogen sources to passivate defective colloidal WS_2 NFs with I-, Br-, and Cl-, respectively. WS_2 NF passivated with Br^- (WS_2-Br NFs) ions has been adopted as reference sample due to the intermediate atomic radius of Br^-, however similar results has been obtained with I^- and Cl^-, which are shown in the Supporting Information sections 'Passivation of WS_2 nanoflakes with I^- ions' and 'Passivation of WS_2 nanoflakes with Cl^- ions', respectively.

UV-Vis absorption spectra of pristine and Br^- passivated colloidal WS_2 NFs are reported in Figure 1b. Similarly to WS_2-Br NFs, the pristine sample was sonicated in NMF without methylammonium halide salts in order to exclude any effects of sonication on the WS_2 NF properties. We immediately observe a marked difference in the color of the solution of pristine and halide passivated colloidal WS_2 NFs. The diluted solution of pristine WS_2 NFs appears deep taupe, while the WS_2-Br is orange-reddish (inset in Figure 1b). The optical absorption of pristine WS_2 NFs is characterized by a broad band in the spectral range between 340 nm and 700 nm without specific optical features, (Figure 1b, blue line). Such behavior is characteristic for WS_2 nanosheets comprising both semiconducting 2H and metallic 1T or 1T' crystal phases,[19] as the pristine WS_2 NFs used here, even though an effect of the large density of defect states on the optical properties cannot be excluded.[44] By contrast, the UV-

Vis absorption spectra of halide passivated NFs have two clear absorption peaks located at 340 nm and 510 nm (Figure 1b, orange line). After a prolonged sonication (42h, see Figure S2), a weak absorption band at around 440 nm along with an overall broadening of the absorption features are observed, which we attribute to an excess of halide atoms included in the crystal structure or to an overall damage of the nanocrystals under prolonged sonication, both detrimental for optical properties. According to previous reports, the absorption spectrum of semiconducting 2H WS_2 monolayer features two absorption peaks (labelled A and B) arising from two transitions at the K/K′ points, related to the strong spin-orbit coupling that induces a valence band splitting of ~0.35 eV. A third strong absorption peak (C) at higher energies originates from interband optical transitions across the bandgap.[22,45,46] We correlate the absorption peaks at 510 and 340 nm to transitions A and C, while the lack of well-defined peaks in the optical region where we expected the transition B, (i.e. between A and C), suggests an overlap of several spectral features that hide the B peak.

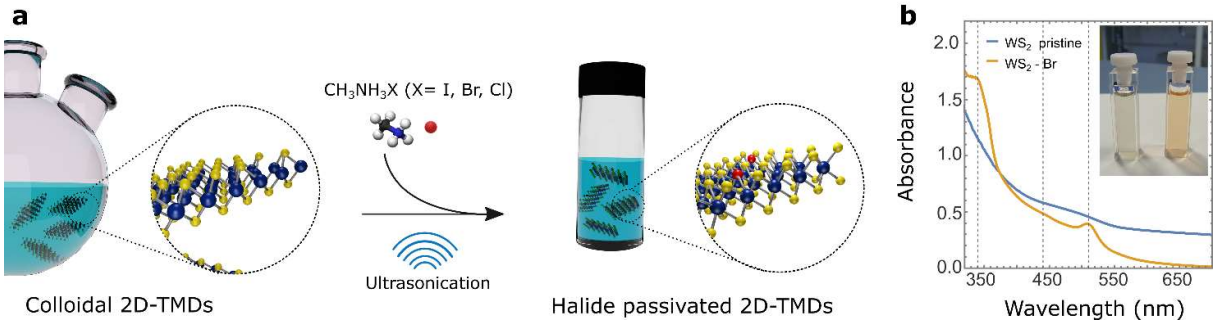

Figure 1. Halide passivation of colloidal WS_2 NFs (a) Schematic illustration of the halide passivation on WS_2 NFs. (b) UV−vis absorption spectra of pristine and Br^- passivated WS_2 NFs after 24 h of sonication and (inset) picture of (left) pristine and (right) Br^- passivated WS_2 NFs solutions.

Optical transitions for our WS_2 NFs result blue-shifted compared to what reported in literature for monolayered sheets with lateral size in the micrometre range, but are consistent with 2D-TMDs nanostructures with lower dimensionality.[17,47–50] Furthermore, WS_2-Br NFs excitonic features result broader than absorption peaks usually observed in mechanically exfoliated WS_2, which could be in part due to the collective contribution from several WS_2 NFs randomly oriented in the solution. The

significant variation in the optical response of WS_2-Br NFs compared to the pristine one suggests that halide treatment could affect one or more of the parameters that directly determine the optical properties of 2D-TMDs, including density of defect states, thickness and crystal structure of nanoflakes. Low-magnification TEM imaging of both the pristine sample (Figure 2a-b) and halide passivated WS_2 NFs (Figure 2b-c) shows that WS_2 NFs are organized in bundles randomly oriented with respect to the TEM grid. A similar morphology has been observed independently of the duration of sonication step (Figure S3); this suggests that morphology is not affected by the treatment. The corresponding selected-area electron diffraction (SAED) image for pristine and WS_2-Br NFs are shown in Figure 2e-f and the SAED patterns are reported in Figure 2g. The SAED patterns of pristine and Br^- passivated colloidal WS_2 NFs are similar demonstrating that the crystal structure is mostly retained after the treatment, although we cannot exclude slight variations that cannot be detected with SAED. Investigation of such minor variation in crystal structure following halide treatment require further detailed atomic-level structural characterization that are out of the scope of our work. The chemical composition of the colloidal halide passivated WS_2 NFs have been analyzed by high angular dark field scanning transmission electron microscopy (HAADF-STEM) combined with energy dispersive X-ray spectrometry (EDX). The HAADF-STEM image in Figure 2h confirms that the morphology of the WS_2 NFs is retained after the treatment, in particular the bundled structure of the NFs can be observed. W and S atoms are detected, and the stoichiometry of the WS_2 NFs is determined to be ~1:1.4 supporting the high density of sulfur vacancies in the pristine sample (see Figure S4 and Table S1). At the same time, the elemental mapping reveals the presence of Br content in Br^- passivated WS_2 NFs samples, confirming that Br is homogenously distributed on the entire NF area (Figure 2m).

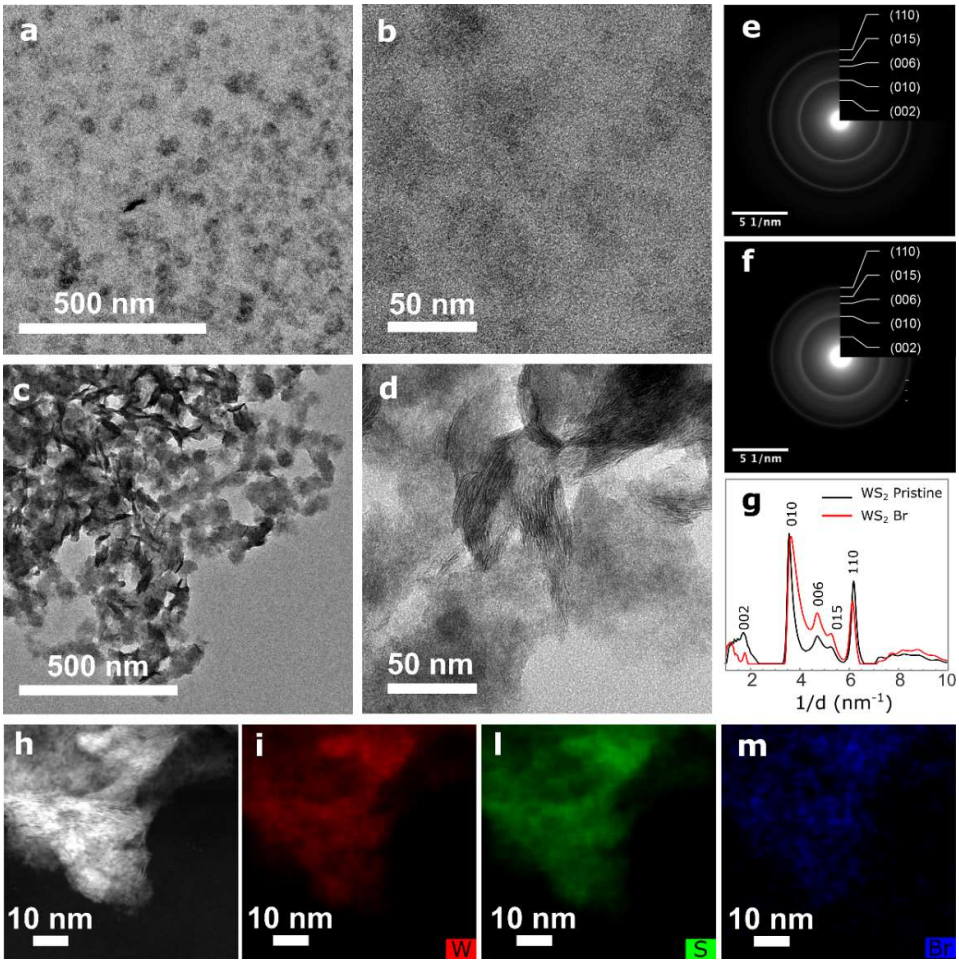

Figure 2. Morphology and composition analyses of pristine and Br^- passivated WS_2 NFs. TEM images of (a-b) pristine and (c-d) Br^- passivated WS_2 NFs. SAED of (e) pristine and (f) Br^- passivated WS_2 NFs. (g) SAED pattern of pristine and Br^- passivated WS_2 NFs. (h) HAADF-STEM image of the WS_2-Br NFs with the corresponding elemental EDX maps for (i) W, (l) S and (m) Br.

To further support the effectiveness of halide passivation, we compared the EDX spectra of the pristine and halide passivated WS_2 NFs sample (Figure S5). The spectra prove the presence of Br atoms on the WS_2-Br NFs, which is quantified in an atomic percentage of 3.9% (see Table S1). The EDX spectra does not allow to discriminate between the Br bound to the surface or intercalated, but according to the observed variation in optical properties we exclude the simple Br intercalation as the main mechanism.

Localized states in halide passivated WS_2 nanoflakes

In order to understand the effectiveness of the halide passivation strategy in suppressing deep gap states, we measured room temperature PL emission from halide passivated WS_2 NFs. As-synthesized defective WS_2 NFs show nearly zero-value PL emission, thus preventing any investigation on the electronic bands through PL measurements. When colloidal WS_2 NFs are passivated with halide atoms, a noticeable PL in the blue-green region (with PLQY of about 1%) emerges thus proving the reduction of density of deep gap states that otherwise would act as ultrafast non-radiative recombination centers. Interestingly, halide passivated WS_2 NFs are highly stable preserving colloidal stability and PL emission after several weeks of storing in ambient atmosphere (Figure S6). From the analysis of the emission spectra of passivated WS_2 NFs, we clearly detect an excitation-wavelength-dependent behavior of PL. The emission spectrum, which consists of distinctive emission features, shifts toward longer wavelengths with the increasing excitation wavelength (Figure 3a). Similar behavior has been observed in liquid exfoliated WS_2 quantum dots due to the polydispersity of the sample that affect the PL wavelength emission because of lateral confinement effects.[51] However, the well-defined absorption bands in the absorption spectra and the presence of distinctive features in a single PL spectrum suggests the presence of localized electronic states, which favor the exciton recombination process (see schematic in Figure 3b).[52]

In order to probe the spectral origin of the observed emitting states, we perform photoluminescence excitation (PLE) spectroscopy. Figure 3c-d shows the PLE intensity maps of halide-passivated WS_2 NFs after 24h of sonication along with the PLE spectra at relevant detection wavelength. PLE map highlights three main high-intensity emission signals at 430 nm, 490 nm and 530 nm resulting from excitation wavelength of about 380 nm, 430 nm, 470 nm. The PLE spectra, extracted from PLE map in correspondence of high intensity emission signals are substantially different from absorption spectra, discussed above.

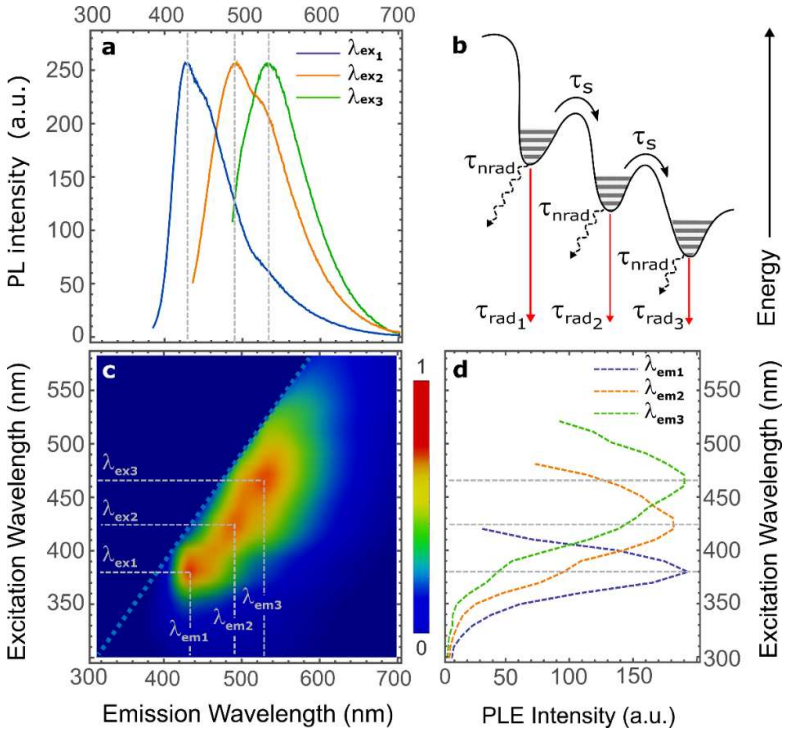

Figure 3. Photoluminescence from Br^- passivated WS_2 NFs. (a) PL spectra of Br^- passivated WS_2 NFs at excitation wavelengths of 380 nm (λex_1), 430 nm (λex_2), and 470 nm (λex_3). (b) Schematic of the competing relaxation pathways in halide passivated WS_2 NFs. High excitation energies allow charge carriers to access to high-lying localized states from which recombine competing with intervalley scattering and bandgap emission. (c) PLE intensity map. (d) PLE spectra extracted from PLE maps at detection wavelength corresponding to stronger PL emission signals (λem_1=430 nm, λem_2=490 nm and λem_1=530 nm).

Absorption spectra shows only two absorption peaks and a broad absorption between them, while PLE spectra exhibit distinct peaks providing more information for the study of absorption transitions and related emissive states. The PLE spectrum excited at 430 nm shows a distinctive enhancement in correspondence with the region of the absorption spectra between A and C peaks, precisely at 380 nm, where the lack of distinct peaks in the absorption spectra hampers the unambiguous match between absorption and emission signals. The PLE spectrum at 490 nm reaches the maximum intensity at about 430 nm and exhibits two less intense additional peaks at 380 nm and 470 nm. Similar situation is observed in the PLE spectrum at 530 nm that has its maximum at 470 nm along

with less intense features at 380 nm, 430 nm, and 510 nm, the last one in correspondence with the A transition in the absorption spectrum.

All the above measurements suggest that exciton recombination in halide passivated WS_2 NFs is strongly influenced by localized states related to surface mediated processes. The emissive features stem from surface states introduced by halide passivation that compete with intervalley scattering and bandgap emission. In particular, when the samples are excited at high excitation energies, the probability for charge carriers to access and to couple to high-lying states is very high. As a result, the emission from the A band is significant only for excitation wavelength just above the band edge. To further study the PL emission as a function of the excitation wavelength, we investigated the decay dynamics of the exciton states through time-resolved PL (TRPL), with the aim to disentangle the mechanisms involved in radiative recombination. TRPL maps obtained with excitation wavelengths of 380 nm, 430 and 470 nm and relative PL decay spectra under the detection wavelength of 530 nm are shown in Figure 4.

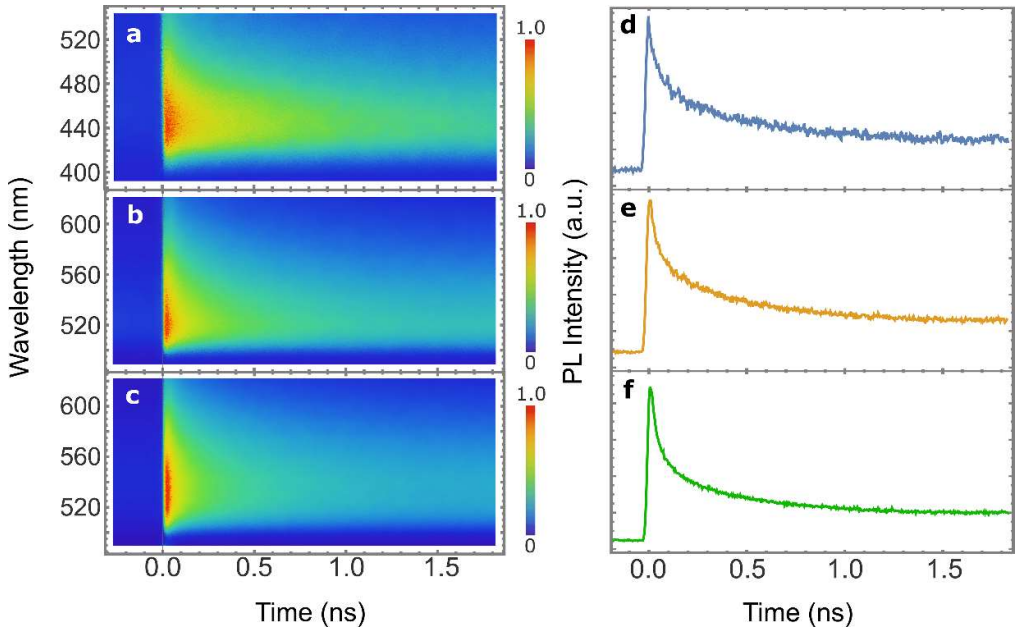

Figure 4. Exciton radiative decay from Br- passivated WS_2 NFs. TRPL emission maps of Br^- passivated WS_2 NFs for excitation wavelength of (a) 380 nm, (b) 430 nm, (c) 470 nm, respectively; and (d-e-f) relative PL decay transients under detection wavelength at 530 nm.

The spectrograms of the exciton states extracted from the TRPL maps reveal non-exponential dynamics, with an initial fast decay in the sub-nanosecond range followed by a slower tail with characteristic time in the order of nanoseconds. This suggests that after photoexcitation, most of the excitons population decay via a very fast non-radiative recombination through the residual defect states at the surface while some long lived charge carriers survives trapped at localized states introduced with halide passivation, which slow down the intervalley relaxation.[52,53] The interpretation is further supported by time-resolved spectrograms obtained at different excitation wavelength, from which it is observed that the decay becomes faster as the excitation wavelength approach the band edge, validating the conclusion of a slow intervalley scattering process mediated by localized states. Analogous results were obtained for WS_2 NFs passivated with I ions (see Figure S9 and Figure S10) and Cl ions (see Figure S13 and Figure S14).

Restoring of electronic band structure of colloidal WS_2 nanoflakes

We used DFT simulations to explore the influence of sulfur vacancies and halide passivation on the electronic structure of WS_2 NFs.[56] Defect free, defective and halide passivated single layer (1L) WS_2 structures modelled by using a 3x3 supercell are illustrated in Figure 5. This relatively small simulation cell is intentionally used to resemble the high defect amount present in the as grown experimental WS_2 samples. The density of states (DOS, panel b) of a defect-free WS_2 monolayer shows a clean band gap without intragap states (maroon line). Note that the simulated band gap for the extended layer results to be 1.6 eV, slightly underestimated with respect to the corresponding experimental value (2.03 eV), as expected by DFT. The latter value is smaller than the optical bandgap (2.43 eV, i.e. 510 nm) measured here for WS_2 NFs, due to the effect of the lateral quantum confinement.[56]

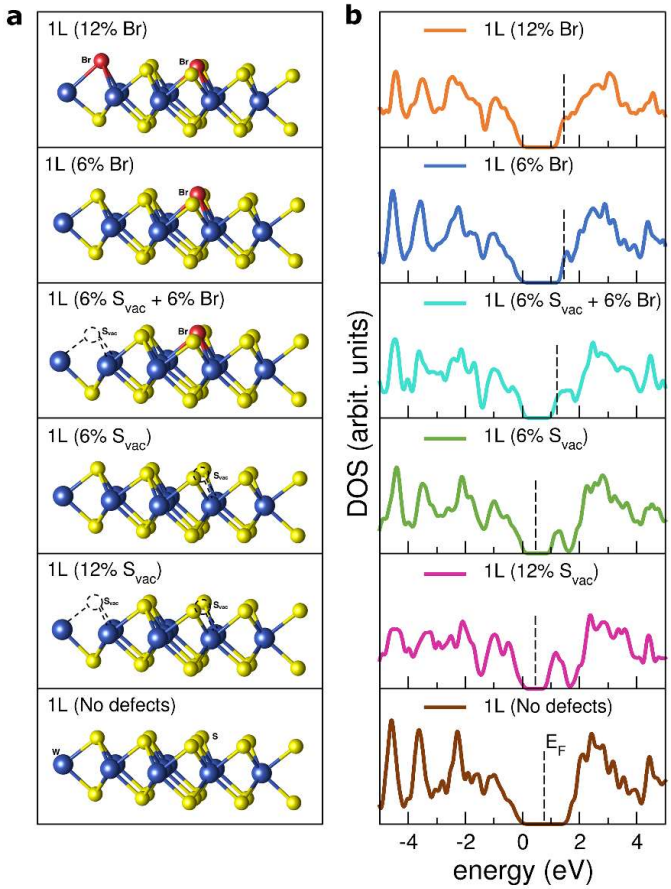

Figure 5. DFT simulations of Br^- passivated WS_2 NFs (a) Modelled defect free, defective and halide passivated WS_2 structures and (b) DOS of the modelled structures.

The presence of one or two sulfur vacancies (Svac) in the 3 × 3 supercell, corresponding to 6% (green line) and 12% (pink line) of S defects, respectively, introduce an intragap state near the conduction band (CB) edge. The creation of one S-vacancy (6%) leaves an empty dangling bond state lying deep in the band gap, which is responsible for the ultrafast non-radiative recombination of photoexcited excitons. Vacancy passivation with halide Br atoms (blue line) saturates the defect state and the band gap of the undefective layer is nearly restored. Br acts as aliovalent substituent that saturates the S vacancy and donates its extra p-electron to the host, occupying the bottom of the WS_2 conduction bands (n-type degenerate doping). Increasing the ratio of the incorporated heteroatoms up to very high content (e.g. 12% Br, orange line) does not significantly change this picture, simply imparting shift of the Fermi level deep within the WS_2 conduction band. Mixed configuration with Svac and Br

ion coexisting in the same sample (e.g. 6% Svac+6% Br, cyan line) exhibit intermediate behavior with the effects of the vacancy and of dopant that sum up giving a reduction of the effective bad gap (shallow S-derived defect state) and occupation of the bottom of the conduction band (Br charge donation). We also have investigated the effect of vacancies and halide passivation on WS_2 in bilayer configuration by performing DFT calculation for electronic structure. In the bilayer regime, we take in consideration also the possible intercalation of halide atoms within the bilayer and possible effects arising from the interaction between intercalated atoms and WS_2 layers. Intercalation of halide atoms does not have dramatic effect on both electronic structure and absorption spectra, while sulfur vacancies and halide passivation have effects on WS_2 bilayer similar to those observed for the monolayer (see Figure S15 and S16).

CONCLUSIONS

We have investigated an effective strategy to passivate chalcogen vacancies of colloidal WS_2 NFs while preserving colloidal stability. Based on EDX and DFT results, we propose that halide ligands bind unsaturated metal cation suppressing deep gap states and nearly restoring the bandgap of defective WS_2 to that of a defect free crystal, which leads to the activation of PL emission. Furthermore, our study reveals that halide passivated WS_2 NFs are characterized by the presence of localized surface states that strongly dictate the excited-state relaxation pathways. Our results support the conclusion that in halide-passivated WS_2 NFs the presence of localized states hinder the intervalley scattering process promoting radiative recombination before relaxation to the band edge. As a consequence, the vast majority of initial excited states recombine before incurring in intervalley scattering, whereas only a small fraction of them relax to the band edge and recombine emitting lower energy photons. Indeed, emission from A transition is significative only for excitation wavelengths just above the band edge because the access to localization site is significantly reduced at lower excitation energy.

In conclusion, our findings reveal the possibility of tailoring optical properties of colloidal 2D-TMDs exploiting solution-phase passivation approaches. In particular, halide passivation neutralizes sulfur vacancies, making WS_2 NFs bright in photoluminescence, and at the same time introduces localized states that affect optical emission, revealing the full relevance to develop similar passivation schemes for a wide range of applications including multicolour biolabeling, display and lasers based on colloidal 2D-TMDs.

ASSOCIATED CONTENT

Supporting Information. Picture of a solution of WS_2-Br NFs; evolution of UV−vis absorption spectra of Br^- passivated WS_2 NFs after 18h, 24 h, and 42 h of sonication; morphological evolution of WS_2-Br NFs after 18h, 24 h, and 42 h of sonication; EDX maps for pristine WS_2 NFs; atomic concentration of the as-synthesized and Br^- passivated WS_2 NFs measured by the quantification of the EDX maps; EDX spectra for the pristine and Br^- passivated WS_2 and NFs; photoluminescence spectra of Br^- passivated WS_2 NFs after several months of storing in air; photophysical and morphological characterization of I^- and Cl^- passivated WS_2 NFs; DFT simulation of defect free, defective and halide passivated WS_2 double layer.

AUTHOR INFORMATION

Corresponding authors

*E-mail: aurora.rizzo@nanotec.cnr.it; Tel.: +39 0832 319816

*E-mail: rosanna.mastria@nanotec.cnr.it; Tel.: +39 0832 319101

Notes

The authors declare no competing interests.

ACKNOWLEDGMENT

A. R., R. M., C. N., and R. S. gratefully acknowledge SIR project "Two-Dimensional Colloidal Metal Dichalcogenides based Energy-Conversion Photovoltaics" (2D ECO), Bando SIR (Scientific Independence of young Researchers) 2014 MIUR Decreto Direttoriale 23 gennaio 2014 no. 197 (project number RBSI14FYVD, CUP: B82I15000950008). The authors gratefully acknowledge Dr Alessandra Quarta and Dr Riccardo Di Corato for fruitful discussions, and Sonia Carallo for technical support. The authors gratefully acknowledge Antonio Gianfrate and Antonio Fieramosca for help with data elaboration.

REFERENCES

(1) Fiori, G.; Bonaccorso, F.; Iannaccone, G.; Palacios, T.; Neumaier, D.; Seabaugh, A.; Banerjee, S. K.; Colombo, L. Electronics Based on Two-Dimensional Materials. *Nat. Nanotechnol.* **2014**, *9*, 768.

(2) Mak, K. F.; Shan, J. Photonics and Optoelectronics of 2D Semiconductor Transition Metal Dichalcogenides. *Nat. Photonics* **2016**, *10*, 216.

(3) Manzeli, S.; Ovchinnikov, D.; Pasquier, D.; Yazyev, O. V; Kis, A. 2D Transition Metal Dichalcogenides. *Nat. Rev. Mater.* **2017**, *2*, 17033.

(4) Mueller, T.; Malic, E. Exciton Physics and Device Application of Two-Dimensional Transition Metal Dichalcogenide Semiconductors. *npj 2D Mater. Appl.* **2018**, *2* (1), 29.

(5) Voiry, D.; Mohite, A.; Chhowalla, M. Phase Engineering of Transition Metal Dichalcogenides. *Chem. Soc. Rev.* **2015**, *44* (9), 2702–2712.

(6) Ryder, C. R.; Wood, J. D.; Wells, S. A.; Hersam, M. C. Chemically Tailoring Semiconducting Two-Dimensional Transition Metal Dichalcogenides and Black Phosphorus. *ACS Nano* **2016**, *10* (4), 3900–3917.

(7) Li, X.-L.; Han, W.-P.; Wu, J.-B.; Qiao, X.-F.; Zhang, J.; Tan, P.-H. Layer-Number Dependent Optical Properties of 2D Materials and Their Application for Thickness Determination. *Adv. Funct. Mater.* **2017**, *27* (19), 1604468.

(8) Bertolazzi, S.; Gobbi, M.; Zhao, Y.; Backes, C.; Samorì, P. Molecular Chemistry Approaches for Tuning the Properties of Two-Dimensional Transition Metal Dichalcogenides. *Chem. Soc. Rev.* **2018**, *47* (17), 6845–6888.

(9) Han, J. H.; Kwak, M.; Kim, Y.; Cheon, J. Recent Advances in the Solution-Based Preparation of Two-Dimensional Layered Transition Metal Chalcogenide Nanostructures. *Chem. Rev.* **2018**, *118* (13), 6151–6188.

(10) Hu, G.; Kang, J.; Ng, L. W. T.; Zhu, X.; Howe, R. C. T.; Jones, C. G.; Hersam, M. C.; Hasan, T. Functional Inks and Printing of Two-Dimensional Materials. *Chem. Soc. Rev.* **2018**, *47* (9), 3265–3300.

(11) Kelly, A. G.; Hallam, T.; Backes, C.; Harvey, A.; Esmaeily, A. S.; Godwin, I.; Coelho, J.; Nicolosi, V.; Lauth, J.; Kulkarni, A.; et al. All-Printed Thin-Film Transistors from Networks of Liquid-Exfoliated Nanosheets. *Science* **2017**, *356* (6333), 69–73.

(12) Mastria, R.; Scarfiello, R.; Altamura, D.; Giannini, C.; Liscio, A.; Kovtun, A.; Bianco, G. V.; Bruno, G.; Grillo, V.; Tavabi, A. H.; et al. In-Plane Aligned Colloidal 2D WS2 Nanoflakes for Solution-Processable Thin Films with High Planar Conductivity. *Sci. Rep.* **2019**, *9* (1), 9002.

(13) Kang, J.; Sangwan, V. K.; Wood, J. D.; Hersam, M. C. Solution-Based Processing of Monodisperse Two-Dimensional Nanomaterials. *Acc. Chem. Res.* **2017**, *50* (4), 943–951.

(14) Backes, C.; Higgins, T. M.; Kelly, A.; Boland, C.; Harvey, A.; Hanlon, D.; Coleman, J. N. Guidelines for Exfoliation, Characterization and Processing of Layered Materials Produced by Liquid Exfoliation. *Chem. Mater.* **2017**, *29* (1), 243–255.

(15) Nasilowski, M.; Mahler, B.; Lhuillier, E.; Ithurria, S.; Dubertret, B. Two-Dimensional Colloidal Nanocrystals. *Chem. Rev.* **2016**, *116* (18), 10934–10982.

(16) Jeong, S.; Yoo, D.; Jang, J.; Kim, M.; Cheon, J. Well-Defined Colloidal 2-D Layered Transition-Metal Chalcogenide Nanocrystals via Generalized Synthetic Protocols. *J. Am. Chem. Soc.* **2012**, *134* (44), 18233–18236.

(17) Jin, H.; Ahn, M.; Jeong, S.; Han, J. H.; Yoo, D.; Son, D. H.; Cheon, J. Colloidal Single-Layer Quantum Dots with Lateral Confinement Effects on 2D Exciton. *J. Am. Chem. Soc.* **2016**, *138* (40), 13253–13259.

(18) Yoo, D.; Kim, M.; Jeong, S.; Han, J.; Cheon, J. Chemical Synthetic Strategy for Single-Layer Transition-Metal Chalcogenides. *J. Am. Chem. Soc.* **2014**, *136* (42), 14670–14673.

(19) Mahler, B.; Hoepfner, V.; Liao, K.; Ozin, G. A. Colloidal Synthesis of 1T-WS_2 and 2H-WS_2 Nanosheets: Applications for Photocatalytic Hydrogen Evolution. *J. Am. Chem. Soc.* **2014**, *136* (40), 14121–14127.

(20) Sokolikova, M. S.; Sherrell, P. C.; Palczynski, P.; Bemmer, V. L.; Mattevi, C. Direct Solution-Phase Synthesis of 1T' WSe_2 Nanosheets. *Nat. Commun.* **2019**, *10* (1), 712.

(21) Schiettecatte, P.; Geiregat, P.; Hens, Z. Ultrafast Carrier Dynamics in Few-Layer Colloidal Molybdenum Disulfide Probed by Broadband Transient Absorption Spectroscopy. *J. Phys. Chem. C* **2019**, *123*, acs.jpcc.9b01494.

(22) Zhao, W.; Ghorannevis, Z.; Chu, L.; Toh, M.; Kloc, C.; Tan, P.-H.; Eda, G. Evolution of Electronic Structure in Atomically Thin Sheets of WS_2 and WSe_2. *ACS Nano* **2013**, *7* (1), 791–797.

(23) Mak, K. F.; Lee, C.; Hone, J.; Shan, J.; Heinz, T. F. Atomically Thin MoS_2: A New Direct-

Gap Semiconductor. *Phys. Rev. Lett.* **2010**, *105* (13), 136805.

(24) Zhang, Y.; Chang, T.-R.; Zhou, B.; Cui, Y.-T.; Yan, H.; Liu, Z.; Schmitt, F.; Lee, J.; Moore, R.; Chen, Y.; et al. Direct Observation of the Transition from Indirect to Direct Bandgap in Atomically Thin Epitaxial $MoSe_2$. *Nat. Nanotechnol.* **2013**, *9*, 111.

(25) Sun, Y.; Wang, D.; Shuai, Z. Indirect-to-Direct Band Gap Crossover in Few-Layer Transition Metal Dichalcogenides: A Theoretical Prediction. *J. Phys. Chem. C* **2016**, *120* (38), 21866–21870.

(26) Lezama, I. G.; Arora, A.; Ubaldini, A.; Barreteau, C.; Giannini, E.; Potemski, M.; Morpurgo, A. F. Indirect-to-Direct Band Gap Crossover in Few-Layer $MoTe_2$. *Nano Lett.* **2015**, *15* (4), 2336–2342.

(27) Laturia, A.; Van de Put, M. L.; Vandenberghe, W. G. Dielectric Properties of Hexagonal Boron Nitride and Transition Metal Dichalcogenides: From Monolayer to Bulk. *npj 2D Mater. Appl.* **2018**, *2* (1), 6.

(28) Wang, H.; Zhang, C.; Rana, F. Ultrafast Dynamics of Defect-Assisted Electron–Hole Recombination in Monolayer MoS_2. *Nano Lett.* **2015**, *15* (1), 339–345.

(29) Wang, H.; Zhang, C.; Rana, F. Surface Recombination Limited Lifetimes of Photoexcited Carriers in Few-Layer Transition Metal Dichalcogenide MoS_2. *Nano Lett.* **2015**, *15* (12), 8204–8210.

(30) Thomson, J. W.; Nagashima, K.; Macdonald, P. M.; Ozin, G. A. From Sulfur−Amine Solutions to Metal Sulfide Nanocrystals: Peering into the Oleylamine−Sulfur Black Box. *J. Am. Chem. Soc.* **2011**, *133* (13), 5036–5041.

(31) Pandey, M.; Rasmussen, F. A.; Kuhar, K.; Olsen, T.; Jacobsen, K. W.; Thygesen, K. S. Defect-

Tolerant Monolayer Transition Metal Dichalcogenides. *Nano Lett.* **2016**, *16* (4), 2234–2239.

(32) Li, L.; Long, R.; Bertolini, T.; Prezhdo, O. V. Sulfur Adatom and Vacancy Accelerate Charge Recombination in MoS_2 but by Different Mechanisms: Time-Domain Ab Initio Analysis. *Nano Lett.* **2017**, *17* (12), 7962–7967.

(33) Van Tuan, D.; Dery, H. Localization-Induced Optical Properties of Monolayer Transition-Metal Dichalcogenides. **2019**, 1–24, arXiv:1904.04959.

(34) Roy, S.; Choi, W.; Jeon, S.; Kim, D.-H.; Kim, H.; Yun, S. J.; Lee, Y.; Lee, J.; Kim, Y.-M.; Kim, J. Atomic Observation of Filling Vacancies in Monolayer Transition Metal Sulfides by Chemically Sourced Sulfur Atoms. *Nano Lett.* **2018**, *18* (7), 4523–4530.

(35) Han, H. V.; Lu, A. Y.; Lu, L. S.; Huang, J. K.; Li, H.; Hsu, C. L.; Lin, Y. C.; Chiu, M. H.; Suenaga, K.; Chu, C. W.; et al. Photoluminescence Enhancement and Structure Repairing of Monolayer MoSe2by Hydrohalic Acid Treatment. *ACS Nano* **2016**, *10* (1), 1454–1461.

(36) Wang, R.; Shang, Y.; Kanjanaboos, P.; Zhou, W.; Ning, Z.; Sargent, E. H. Colloidal Quantum Dot Ligand Engineering for High Performance Solar Cells. *Energy Environ. Sci.* **2016**, *9* (4), 1130–1143.

(37) Boles, M. A.; Ling, D.; Hyeon, T.; Talapin, D. V. The Surface Science of Nanocrystals. *Nat. Mater.* **2016**, *15* (2), 141–153.

(38) Ghosh, S.; Manna, L. The Many "Facets" of Halide Ions in the Chemistry of Colloidal Inorganic Nanocrystals. *Chem. Rev.* **2018**, *118* (16), 7804–7864.

(39) Zhang, H.; Jang, J.; Liu, W.; Talapin, D. V. Colloidal Nanocrystals with Inorganic Halide, Pseudohalide, and Halometallate Ligands. *ACS Nano* **2014**, *8* (7), 7359–7369.

(40) Seo, J. W.; Jun, Y. W.; Park, S. W.; Nah, H.; Moon, T.; Park, B.; Kim, J. G.; Kim, Y. J.; Cheon,

J. Two-Dimensional Nanosheet Crystals. *Angew. Chemie - Int. Ed.* **2007**, *46* (46), 8828–8831.

(41) Dirin, D. N.; Dreyfuss, S.; Bodnarchuk, M. I.; Nedelcu, G.; Papagiorgis, P.; Itskos, G.; Kovalenko, M. V. Lead Halide Perovskites and Other Metal Halide Complexes As Inorganic Capping Ligands for Colloidal Nanocrystals. *J. Am. Chem. Soc.* **2014**, *136* (18), 6550–6553.

(42) Dong, A.; Ye, X.; Chen, J.; Kang, Y.; Gordon, T.; Kikkawa, J. M.; Murray, C. B. A Generalized Ligand-Exchange Strategy Enabling Sequential Surface Functionalization of Colloidal Nanocrystals. *J. Am. Chem. Soc.* **2011**, *133* (4), 998–1006.

(43) Ogilvie, S. P.; Large, M. J.; Fratta, G.; Meloni, M.; Canton-Vitoria, R.; Tagmatarchis, N.; Massuyeau, F.; Ewels, C. P.; King, A. A. K.; Dalton, A. B. Considerations for Spectroscopy of Liquid-Exfoliated 2D Materials: Emerging Photoluminescence of N-Methyl-2-Pyrrolidone. *Sci. Rep.* **2017**, *7* (1), 16706.

(44) Shu, H.; Li, Y.; Niu, X.; Wang, J. Greatly Enhanced Optical Absorption of a Defective MoS_2 Monolayer through Oxygen Passivation. *ACS Appl. Mater. Interfaces* **2016**, *8* (20), 13150–13156.

(45) Kozawa, D.; Kumar, R.; Carvalho, A.; Kumar Amara, K.; Zhao, W.; Wang, S.; Toh, M.; Ribeiro, R. M.; Castro Neto, A. H.; Matsuda, K.; et al. Photocarrier Relaxation Pathway in Two-Dimensional Semiconducting Transition Metal Dichalcogenides. *Nat. Commun.* **2014**, *5*, 1–7.

(46) Beal, A. R.; Knights, J. C.; Liang, W. Y. Transmission Spectra of Some Transition Metal Dichalcogenides. II. Group VIA: Trigonal Prismatic Coordination. *J. Phys. C Solid State Phys.* **1972**, *5* (24), 3540–3551.

(47) Ono, S.; Ogura, T. Anomalous Energy Shift of Laterally Confined Two-Dimensional Excitons. *J. Appl. Phys.* **2018**, *124* (3), 34301.

(48) Han, G. G. D.; Tu, K.-H.; Niroui, F.; Xu, W.; Zhou, S.; Wang, X.; Bulović, V.; Ross, C. A.; Warner, J. H.; Grossman, J. C. Photoluminescent Arrays of Nanopatterned Monolayer MoS_2. *Adv. Funct. Mater.* **2017**, *27* (45), 1703688.

(49) Wei, G.; Czaplewski, D. A.; Lenferink, E. J.; Stanev, T. K.; Jung, I. W.; Stern, N. P. Size-Tunable Lateral Confinement in Monolayer Semiconductors. *Sci. Rep.* **2017**, *7* (1), 3324.

(50) Chikan, V.; Kelley, D. F. Size-Dependent Spectroscopy of MoS_2 Nanoclusters. *J. Phys. Chem. B* **2002**, *106* (15), 3794–3804.

(51) Wu, J.-Y.; Zhang, X.-Y.; Ma, X.-D.; Qiu, Y.-P.; Zhang, T. High Quantum-Yield Luminescent MoS_2 Quantum Dots with Variable Light Emission Created via Direct Ultrasonic Exfoliation of MoS_2 Nanosheets. *RSC Adv.* **2015**, *5* (115), 95178–95182.

(52) Caigas, S. P.; Santiago, S. R. M.; Lin, T.-N.; Lin, C.-A. J.; Yuan, C.-T.; Shen, J.-L.; Lin, T.-Y. Origins of Excitation-Wavelength-Dependent Photoluminescence in WS_2 Quantum Dots. *Appl. Phys. Lett.* **2018**, *112* (9), 092106.

(53) Kaasbjerg, K.; Martiny, J. H. J.; Low, T.; Jauho, A.-P. Symmetry-Forbidden Intervalley Scattering by Atomic Defects in Monolayer Transition-Metal Dichalcogenides. *Phys. Rev. B* **2017**, *96* (24), 241411.

(54) Kastl, C.; Koch, R. J.; Chen, C. T.; Eichhorn, J.; Ulstrup, S.; Bostwick, A.; Jozwiak, C.; Kuykendall, T. R.; Borys, N. J.; Toma, F. M.; et al. Effects of Defects on Band Structure and Excitons in WS2 Revealed by Nanoscale Photoemission Spectroscopy. *ACS Nano* **2019**.

(55) Wang, S.; Lee, G.-D.; Lee, S.; Yoon, E.; Warner, J. H. Detailed Atomic Reconstruction of Extended Line Defects in Monolayer MoS2. *ACS Nano* **2016**, *10* (5), 5419–5430.

(56) Here We Are Interested in the Modification Trend of the Defect State Distribution Due to the

Progressive Saturation of the Sulfur Vacancies by Halide Distribution, Rather than a One-to-One Quantitative Agreement with the Experiments. Thus, the numerical corrections to the electronic properties to recover the experimental values (such as the optical band gap), which would require the simulation of electronic and optical properties at a higher level of theory (e.g. many body GW Bethe Salpeter approaches), goes beyond the aim of this work

(57) Perdew, J. P.; Burke, K.; Ernzerhof, M. Generalized Gradient Approximation Made Simple. *Phys. Rev. Lett.* **1996**, *77* (18), 3865–3868.

(58) Giannozzi, P.; Baroni, S.; Bonini, N.; Calandra, M.; Car, R.; Cavazzoni, C.; Ceresoli, D.; Chiarotti, G. L.; Cococcioni, M.; Dabo, I.; et al. QUANTUM ESPRESSO: A Modular and Open-Source Software Project for Quantum Simulations of Materials. *J. Phys. Condens. Matter* **2009**, *21* (39), 395502.

(59) Dal Corso, A. Projector Augmented Wave Method with Spin-Orbit Coupling: Applications to Simple Solids and Zincblende-Type Semiconductors. *Phys. Rev. B* **2012**, *86* (8), 85135.

(60) Troullier, N.; Martins, J. L. Efficient Pseudopotentials for Plane-Wave Calculations. *Phys. Rev. B* **1991**, *43* (3), 1993–2006.

(61) Grimme, S. Semiempirical GGA-Type Density Functional Constructed with a Long-Range Dispersion Correction. *J. Comput. Chem.* **2006**, *27* (15), 1787–1799.

(62) Colle, R.; Parruccini, P.; Benassi, A.; Cavazzoni, C. Optical Properties of Emeraldine Salt Polymers from Ab Initio Calculations: Comparison with Recent Experimental Data. *J. Phys. Chem. B* **2007**, *111* (11), 2800–2805.

(63) Calzolari, A.; Ruini, A.; Catellani, A. Transparent Conductive Oxides as Near-IR Plasmonic Materials: The Case of Al-Doped ZnO Derivatives. *ACS Photonics* **2014**, *1* (8), 703–709.

Supporting information

Photoluminescence Emission Induced by Localized States in Halide Passivated Colloidal Two-Dimensional WS_2 Nanoflakes

Rosanna Mastria,[1] Anna Loiudice,[2] Jan Vávra,[2] Concetta Nobile,[1] Riccardo Scarfiello,[1] P. Davide Cozzoli,[1,3,4] Nicola Sestu,[5] Daniela Marongiu,[5] Francesco Quochi,[5] Raffaella Buonsanti,[2] Michele Saba,[5] Arrigo Calzolari,[6] Aurora Rizzo[1]**

[1]CNR NANOTEC - Institute of Nanotecnology, Polo di Nanotecnologia, c/o Campus Ecotekne, Via Monteroni, 73100 Lecce, Italy;

[2]Laboratory of Nanochemistry for Energy (LNCE), Department of Chemical Sciences and Engineering, École Polytechnique Fédérale de Lausanne, Sion, CH-1950, Switzerland

[3]Dipartimento di Matematica e Fisica "E. De Giorgi", Università del Salento, Via per Arnesano, 73100 Lecce, Italy.

[4]UdR INSTM di Lecce, c/o, Università del Salento, Campus Ecotekne, via Arnesano, 73100 Lecce, Italy.

[5]Dipartimento di Fisica, Università di Cagliari, I-09042 Monserrato, Italy

[6]Istituto Nanoscienze, CNR-NANO, S3 Center, Via Campi 213/a, 41125 Modena, Italy

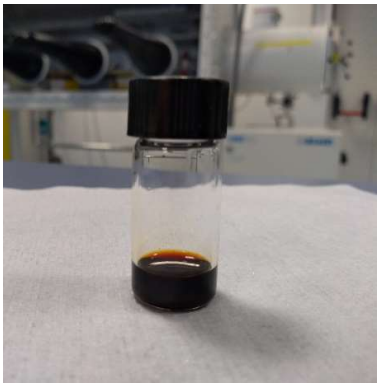

Figure S1. Picture of a 4 mg/ml solution of WS_2-Br NFs in NMF

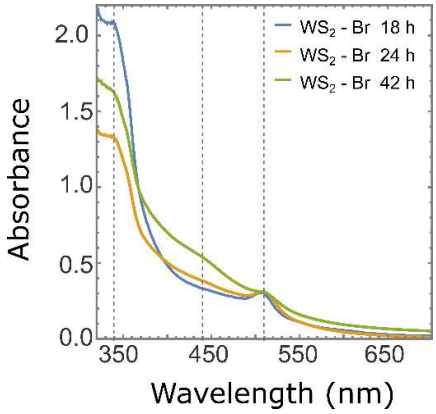

Figure S2. Evolution of UV−vis absorption spectra of Br^- passivated WS_2 NFs after 18h, 24 h, and 42 h of sonication. Each absorption spectrum is normalized by the A exciton peak.

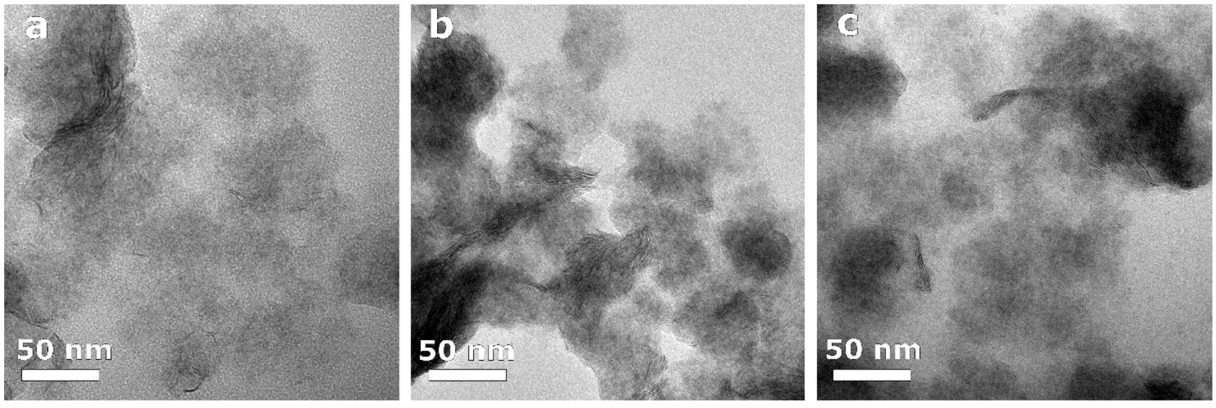

Figure S3. TEM images of WS_2-Br NFs after (a) 18h, (b) 24 h, and (c) 42 h of sonication.

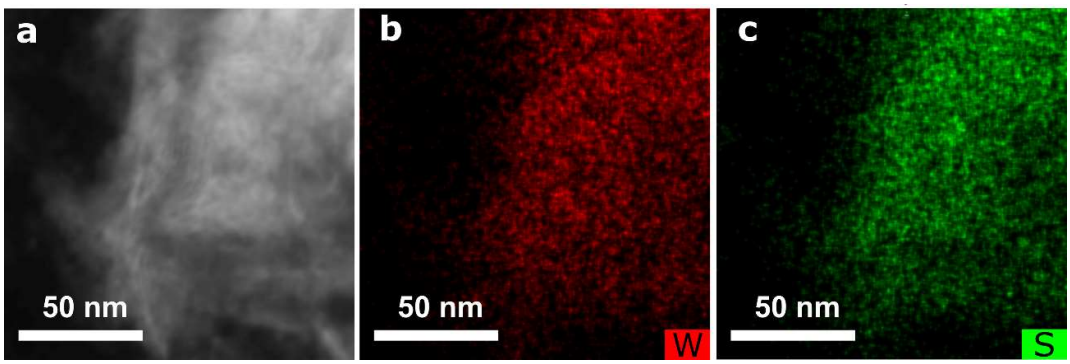

Figure S4. (a) HAADF-STEM image of the WS_2-Br NFs with the corresponding elemental EDX maps for (b) W and (c) S.

	W (at. %)	S (at. %)	Br (at. %)	S : W ratio
Pristine WS_2 NFs	**42.5**	**57.5**	**0**	**1.4**
WS_2 – Br NFs	**37.7**	**58.4**	**3.9**	**1.6**

Table S1. Atomic concentration of the as-synthesized and Br^- passivated WS_2 NFs measured by the quantification of the EDX maps in Supplementary Figure 5. The selected energy transitions for atomic percentage quantification were L= 8.4 eV, K= 2.3 eV, K= 11.9 eV for W, S and Br respectively. The uncertainty on the EDX analysis was estimated to be 3-4%.

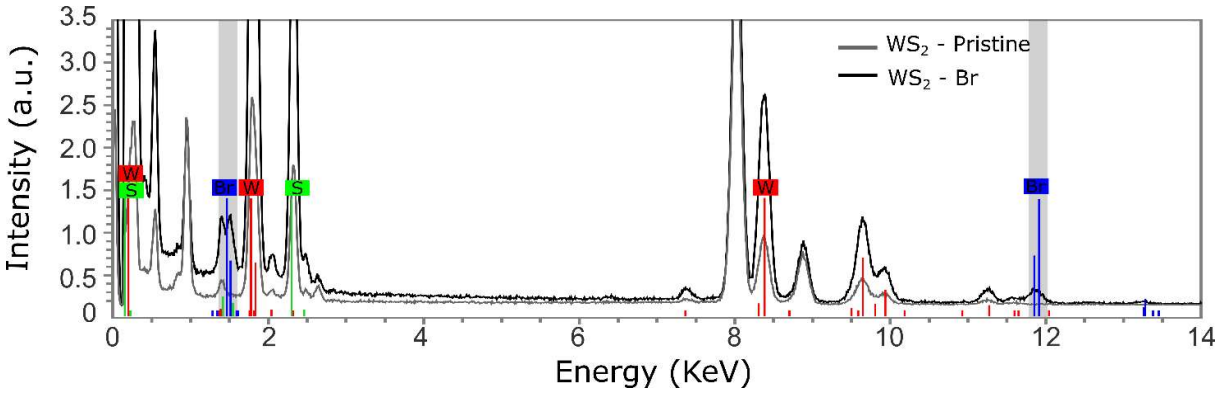

Figure S5. EDX spectra for the pristine and Br^- passivated WS_2 and NFs.

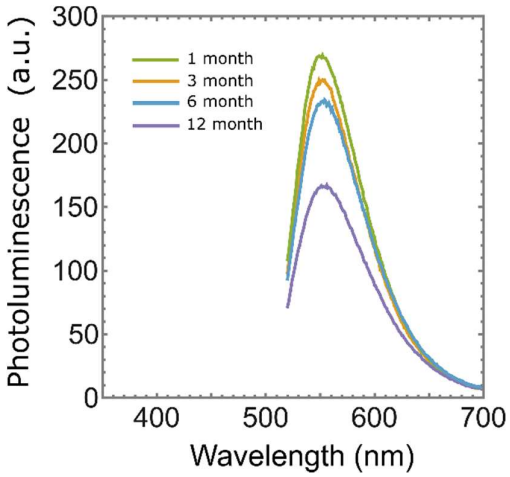

Figure S6. Photoluminescence spectra of Br^- passivated WS_2 NFs after several months of storing in air. We register a significant photoluminesce reduction only after 12 months of air exposure.

Passivation of WS_2 nanoflakes with I^- ions

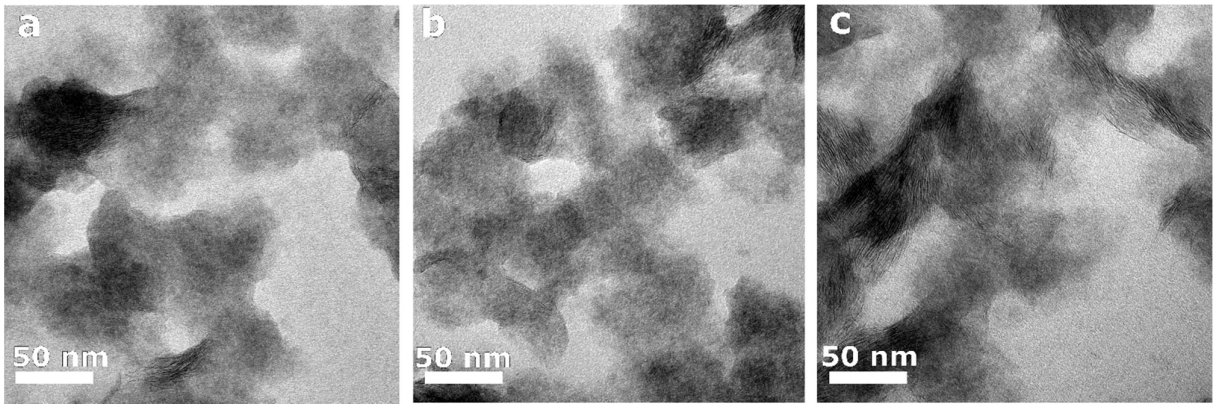

Figure S7. TEM images of WS_2-I NFs after (a) 18h, (b) 24 h, and (c) 42 h of sonication.

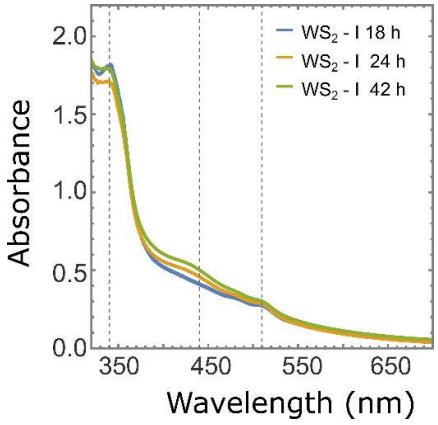

Figure S8. Evolution of UV−vis absorption spectra of I^- passivated WS_2 NFs after 18h, 24 h, and 42 h of sonication

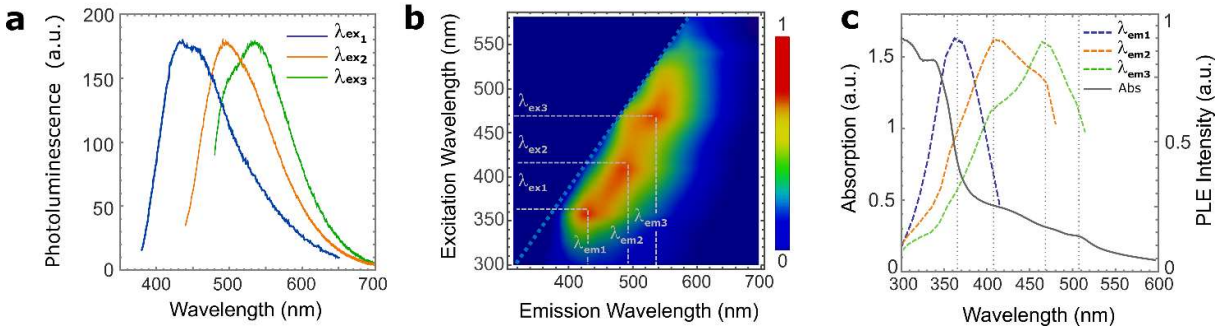

Figure S9. (a) PL spectra of I^- passivated WS_2 NFs at excitation wavelengths of 380 nm (λ_{em1}), 430 nm (λ_{em2}), and 470 nm (λ_{em3}). (b) PLE intensity map. (c) PLE spectra extracted from PLE maps at detection wavelength corresponding to stronger PL emission signals (430 nm, 490 nm and 530 nm). Absorption spectrum is also shown for comparison.

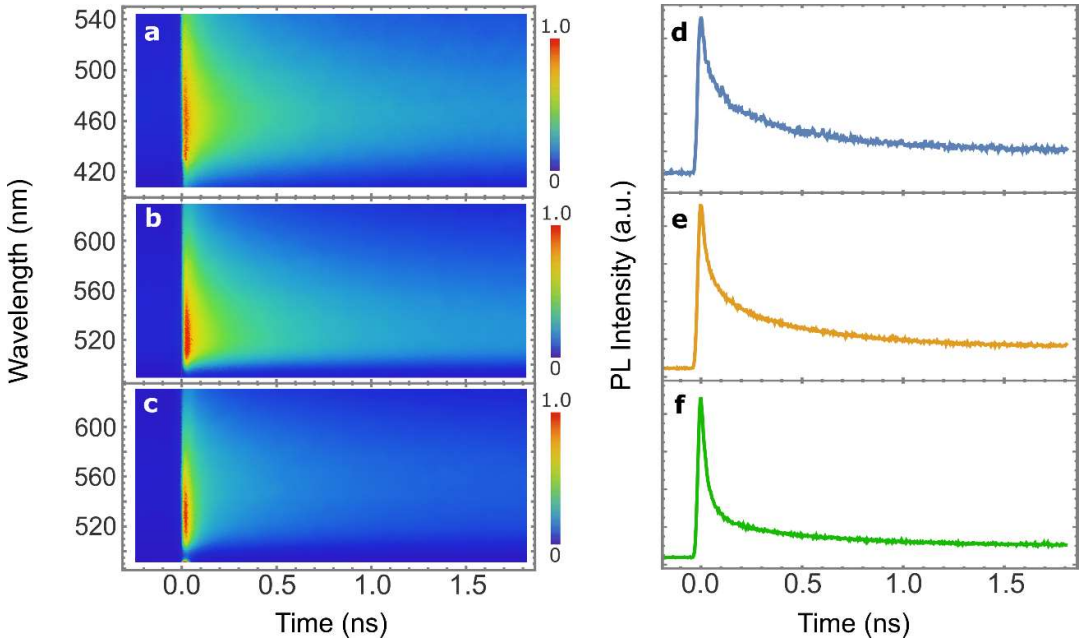

Figure S10. TRPL from I^- passivated WS_2 NFs after 24 h of sonication. (a,b,c) TRPL emission maps of I^- passivated WS_2 NFs for excitation wavelength of 380 nm, 430 nm, 470 nm, respectively; and (d,e,f) relative PL decay transients under detection wavelength at 530 nm.

Passivation of WS_2 nanoflakes with Cl^- ions

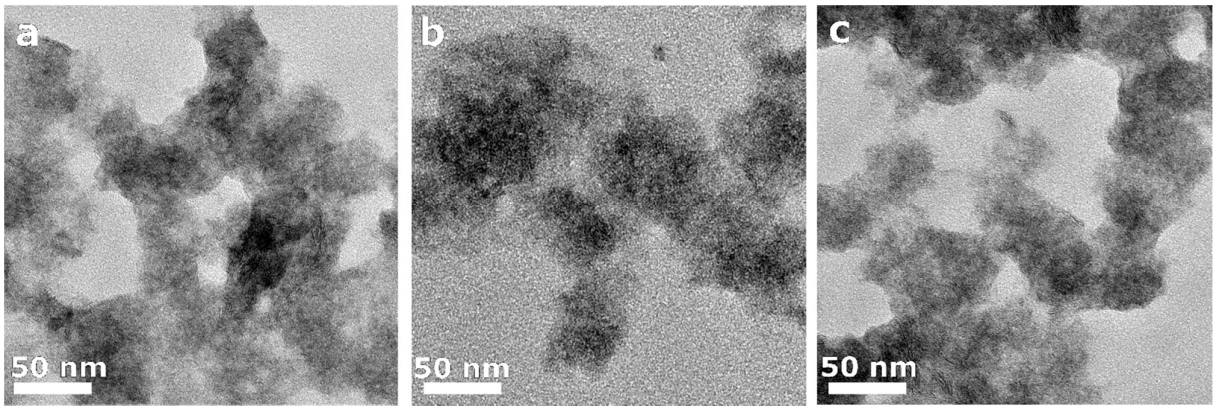

Figure S11. TEM images of WS_2-Cl NFs after (a) 18h, (b) 24 h, and (c) 42 h of sonication.

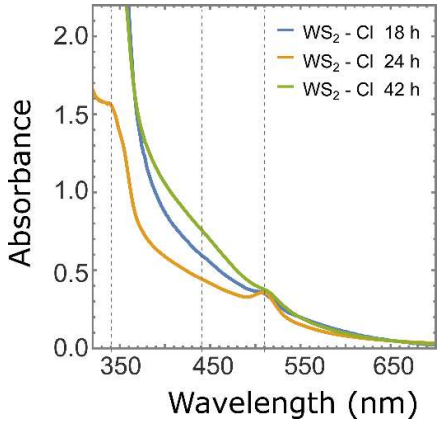

Figure S12. Evolution of UV−vis absorption spectra of Cl^- passivated WS_2 NFs after 18h, 24 h, and 42 h of sonication

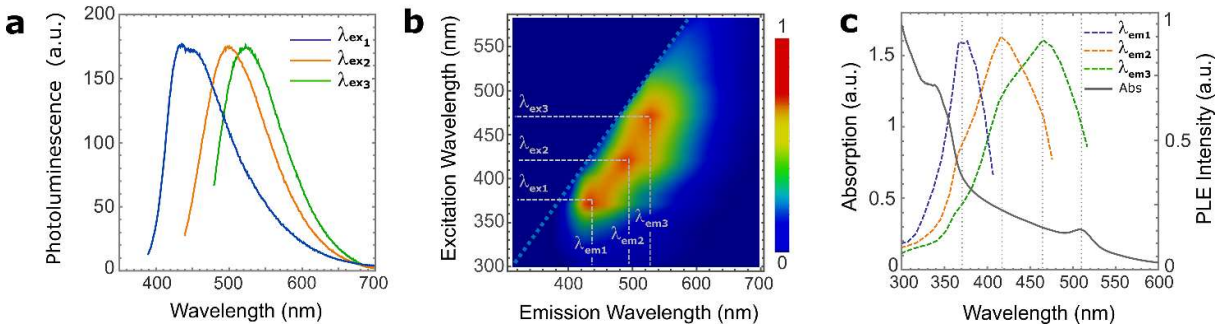

Figure S13. (a) PL spectra of Cl^- passivated WS_2 NFs at excitation wavelengths of 380 nm (λ_{em1}), 430 nm (λ_{em2}), and 470 nm (λ_{em3}). (b) PLE intensity map. (c) PLE spectra extracted from PLE maps at detection wavelength corresponding to stronger PL emission signals (430 nm, 490 nm and 530 nm). Absorption spectrum is also shown for comparison.

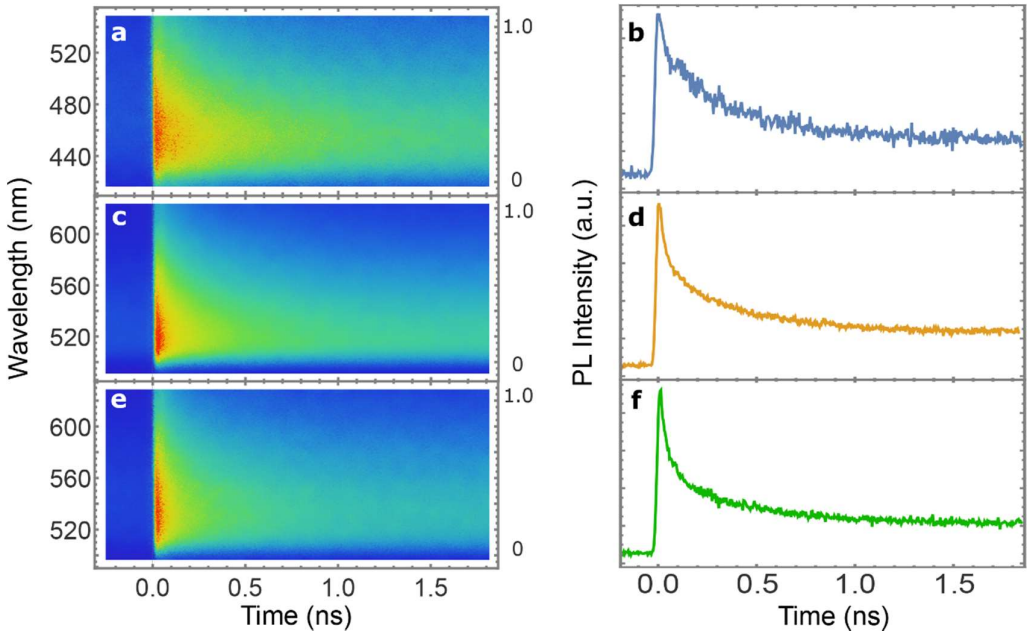

Figure S14. TRPL from Cl^- passivated WS_2 NFs after 24 h of sonication. (a,b,c,) TRPL emission maps of Cl^- passivated WS_2 NFs for excitation wavelength of 380 nm, 430 nm, 470 nm, respectively; and (d,e,f) relative PL decay transients under detection wavelength at 530 nm.

DFT simulations of WS_2 bilayer structures

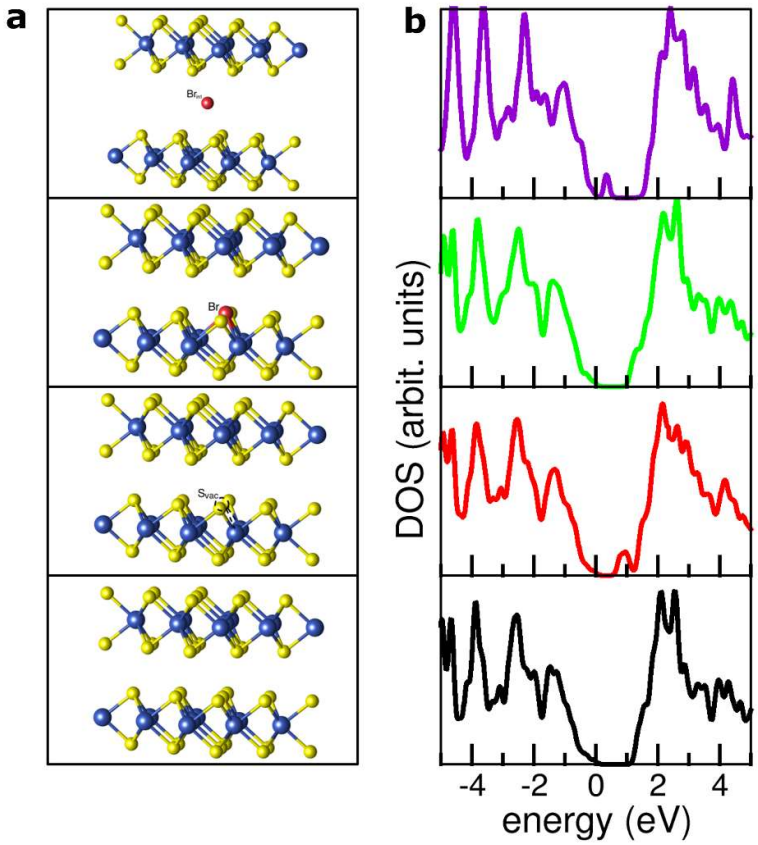

Figure S15. (a) Atomic structure and (b) density of states for WS_2 double layer (2L) with and without a single defect. From bottom to top: no defects; one S vacancy ($1S_{vac}$), one substitutional Br atom (1Br); and one interstitial Br atom ($1Br_{int}$).

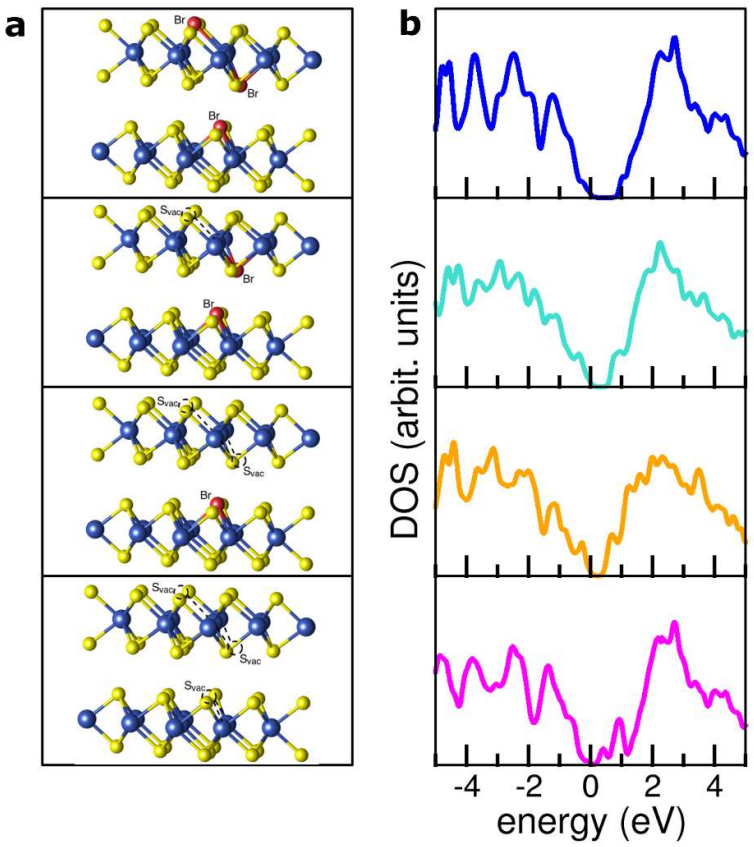

Figure S16. (a) Atomic structure and (b) density of states for WS_2 double layer (2L) with three defects. From bottom to top: three S vacancy ($3S_{vac}$), two S vacancy and one substitutional Br atom ($2S_{vac}$+1Br), one S vacancy and two substitutional Br atoms ($1S_{vac}$+2Br), three substitutional Br atoms (3Br).